ISSN 1288-1619

CNRS - Université Pierre et Marie Curie - Université Versailles-Saint-Quentin
CEA - ORSTOM - Ecole Normale Supérieure - Ecole Polytechnique

Institut Pierre Simon Laplace
des Sciences de l'Environnement Global

Notes du Pôle de Modélisation

The role of sea ice thermodynamics in the Northern Hemisphere climate as simulated by a global coupled ocean-atmosphere model

Y. Le Clainche (1) , P. Braconnot (1) , O. Marti (1) , S. Joussaume (1) , J-L. Dufresne (2) and M-A. Filiberti (3)

(1) IPSL/LSCE - Laboratoire des Sciences du Climat et de l'Environnement, UMR 1572 CEA-CNRS, Orme des Merisiers, 91191 Gif sur Yvette Cedex, France
(2) IPSL/LMD - Laboratoire de Météorologie Dynamique, Université Paris VI, Case 99, 4 place Jussieu, 75252 Paris Cedex 05, France
(3) IPSL / LODYC - Laboratoire d'Océanographie Dynamique et de Climatologie, Université Paris VI, Case 100, 4 place Jussieu, 75252 Paris Cedex 05, France

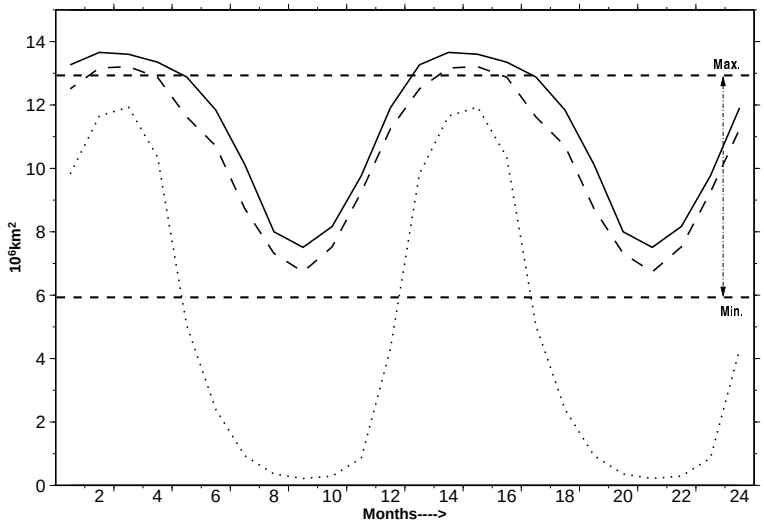

Octobre 2001 **Note n° 21**

I P S L

CNRS - Université Pierre et Marie Curie - Université Versailles-Saint-Quentin
CEA -CNES - ORSTOM - Ecole Normale Supérieure - Ecole Polytechnique

Institut Pierre Simon Laplace
des Sciences de l'Environnement Global

C E T P - LMD - LODYC - LPCM - LSCE - SA

Université Pierre-et-Marie-Curie
B 102 - T15-E5 - 4, Place Jussieu
75252 Paris Cedex 05 (France)
Tél : (33) 01 44 27 39 83
Fax : (33) 01 44 27 37 76

Université Versailles-Saint-Quentin
23 rue du Refuge
78035 Versailles Cedex (France)
Tél : (33) 01 39 25 58 23
Fax : (33) 01 39 25 58 18

We investigate the role of sea ice in the Northern Hemisphere climate as simulated by the IPSL coupled ocean-atmosphere model. A complex thermodynamic parameterization of sea ice has been introduced in this global model. Our study is based on the comparison of a simulation performed with this new version, with an earlier one that only differs by the sea-ice scheme. Our results demonstrate not only the need to include an efficient thermodynamic sea ice model in global coupled ocean-atmosphere models, but also the large impact of the sea ice on the climate system. The thermal inertia of sea-ice plays a role as important as the sea-ice albedo feedback and the insulator effect of sea ice. It needs to be accounted for to get a good representation of the seasonal cycle of sea-ice cover. This inertia is modulated by the heat budgets at the bottom and surface of the ice and by the energy absorbed into leads. In our simulations, the sea-ice has an impact on the atmospheric circulation in the Arctic and North Atlantic and on the hydrological cycle, which strongly affects the surface and thermohaline ocean circulation in the Atlantic. The transport of heat and salt from the North Atlantic to the Norwegian sea and the seasonal ice brine rejection favor the deep convection in the Norwegian sea during the winter. They have a key role in the model and strengthen the ocean equator to pole heat transport.

Octobre 2001 , Note n° 21

Directeur de publication : Jean Jouzel, Directeur de l'IPSL
ISSN 1288-1619

The role of sea ice thermodynamics in the Northern Hemisphere climate as simulated by a global coupled ocean-atmosphere model

Y. Le Clainche[1 (*)], P. Braconnot[1 (*)], O. Marti[1], S. Joussaume[1], J-L. Dufresne[2] and M-A. Filiberti[3]

[1] IPSL/LSCE - Laboratoire des Sciences du Climat et de l'Environnement, UMR 1572 CEA-CNRS, Orme des Merisiers, 91191 Gif sur Yvette Cedex, France

[2] IPSL/LMD - Laboratoire de Météorologie Dynamique, Université Paris VI, Case 99, 4 place Jussieu, 75252 Paris Cedex 05, France

[3] IPSL / LODYC - Laboratoire d'Océanographie Dynamique et de Climatologie, Université Paris VI, Case 100, 4 place Jussieu, 75252 Paris Cedex 05, France

[(*)] Corresponding authors, e-mail : leclain@lsce.saclay.cea.fr or pasb@lsce.saclay.cea.fr

Abstract: We investigate the role of sea ice in the Northern Hemisphere climate as simulated by the IPSL coupled ocean-atmosphere model. A complex thermodynamic parameterization of sea ice has been introduced in this global model. Our study is based on the comparison of a simulation performed with this new version, with an earlier one that only differs by the sea-ice scheme. Our results demonstrate not only the need to include an efficient thermodynamic sea ice model in global coupled ocean-atmosphere models, but also the large impact of the sea ice on the climate system. The thermal inertia of sea-ice plays a role as important as the sea-ice albedo feedback and the insulator effect of sea ice. It needs to be accounted for to get a good representation of the seasonal cycle of sea-ice cover. This inertia is modulated by the heat budgets at the bottom and surface of the ice and by the energy absorbed into leads. In our simulations, the sea-ice has an impact on the atmospheric circulation in the Arctic and North Atlantic and on the hydrological cycle, which strongly affects the surface and thermohaline ocean circulation in the Atlantic. The transport of heat and salt from the North Atlantic to the Norwegian sea and the seasonal ice brine rejection favor the deep convection in the Norwegian sea during the winter. They have a key role in the model and strengthen the ocean equator to pole heat transport.

1. Introduction

Sea ice is a major component of the climate system at high latitudes. It has a strong impact on the coupled interactions between the atmosphere and the ocean (e.g. Van Ypersele 1990). When sea ice is present, the radiative properties of the surface are modified compared to free ocean conditions. Its high albedo (between 0.6 and 0.9) limits the amount of absorbed solar energy at the surface. Short-wave radiation penetrating into sea ice is mainly converted into latent energy, and only a small part can reach the ocean through the thinnest sea ice. The snow and ice surface temperature can drop down to -30^{o}C or less in winter, which contrasts with the relatively warmer sea surface temperature that remains above the seawater freezing point (~ -1.8^{o}C). The surface infrared emission is then reduced from 300 to 200 Wm^{-2} in winter. With its very weak thermal conductivity, sea ice is a very good insulator for the turbulent heat exchanges at the air-sea interface. Latent and sensible heat fluxes are very weak over sea ice, while fluxes of several hundred Wm^{-2} are typically found over open water areas in winter (Smith et al. 1990). A friction with a slowly moving solid (Semtner 1987) replaces wind stresses at the ocean surface. Sea ice intercepts part of the snow precipitation, but its main effect on the hydrological cycle is through brine rejection during its formation and fresh water release during its melting. These processes modify the density of the surface water (Aagaard et al. 1981). In winter, the salinity increase favors the deep convection.

Sea ice variations can have a profound impact on climate change (Rind et al. 1995; Houghton et al. 1996), and need to be introduced into the models used for future or past climate simulations (Vavrus 1999). Therefore, coupled ocean-atmosphere general circulation models (GCM) have to include a pertinent parameterization of sea ice and of its interaction with the ocean and the atmosphere to simulate properly the high latitude climate (Van Ypersele 1990). The parameterization of sea ice in climate models has evolved towards an interactive climatic component. According to the CMIP (Coupled Model Intercomparison Project) database, approximately 2/3 of the 19 CMIP coupled models represent only the thermodynamic processes (Cubash et al. 1992; Moore and Gordon 1994; Murphy 1994). For most of them the ice thickness is represented by a

single layer (Johns et al. 1997) and the different ice types are not separated. The dynamic processes are represented in only 1/3 of the models (Lunkeit et al. 1996), and half of them use a simple "free drift" model (Manabe and Stouffer 1994). Moreover, half of these 19 coupled climate models use flux correction at the air-sea interface (Cubash et al. 1992; Manabe and Stouffer 1994; Murphy 1994) to prevent climatic drift. Finally, only the last version of the NCAR coupled model uses both complex thermodynamic and dynamic sea ice, without flux correction (Weatherly et al. 1998).

These climate models have been mainly used to simulate the transient response of climate to the gradual increase of carbon dioxide, or to focus on the tropical variability. Some studies with only a slab ocean (Rind et al. 1995) or with a global ocean model (Washington and Meehl 1996) have shown a great sensitivity of sea ice to the climate warming with a dramatic reduction of the Arctic sea ice cover. However, no specific study has been achieved with a global coupled model in order to evaluate how the parameterization of sea ice can affect the model results.

The main objective of the present paper is to analyze the impact of the representation of sea ice thermodynamics on the Northern Hemisphere climate as simulated by a global coupled model. We consider a simulation with the IPSL_CM1 (Institut Pierre Simon Laplace) coupled ocean-atmosphere model into which a complex thermodynamic sea ice model has been recently introduced. To better emphasize the role of sea-ice in the ocean-atmosphere interaction at the seasonal time scale, we compare the results of this simulation with those of a simulation with the previous version of the model (Braconnot et al. 2000) where sea-ice thermodynamics was simplified and the climate of the Arctic not well reproduced. Sea-ice parameterization is the only difference between the two simulations. We investigate not only the role of sea ice on the seasonal cycle of the surface heat fluxes, but also its active role in the oceanic and atmospheric circulation of the Northern Hemisphere. The impact of sea-ice processes on the deep-water formation in the North Atlantic is also emphasized.

The coupled model, the sea ice parameterizations, and the coupling procedures are described in section 2. The results are discussed in the four following sections. The section 3 presents on the one hand the initialization and the spin-up of the simulation and on the other hand the simulated sea ice cover. In section 4 we focus on the relationships between the seasonal cycle of the heat fluxes at the surface, the sea-ice cover and the surface temperature in the Arctic Ocean. The mean hydrology of the Arctic basin and its connection with the North Atlantic are discussed in the section 5. The section 6 show the interaction between deep-water formation and the thermohaline circulation in the ocean. .

2. The coupled model

a. The atmosphere and ocean components

The coupled model is the low-resolution version of the IPSL-CM1 (Institut Pierre et Simon Laplace) coupled model described in Braconnot et al. (1997, 2000).

The atmospheric component is the version 5.3 of the Laboratoire de Météorologie Dynamique (LMD) grid point atmospheric general circulation model (Sadourny and Laval 1984; Harzallah and Sadourny 1995). The resolution is 64 points in longitude, 50 points in sine of the latitude, and 11 vertical sigma levels. At the surface, momentum and heat fluxes are computed separately for sea-ice and open water fractions, using different drag coefficients over ice and ocean (Braconnot et al. *2000*).

The oceanic component is the primitive equation model OPA developed at the

Laboratoire d'Océanographie Dynamique et de Climatologie (LODYC) (Andrich et al. 1988; Delecluse et al. 1993). The horizontal mesh is orthogonal and curvilinear on the sphere. The configuration is geographical in the Southern Hemisphere, but the northern point of convergence has been shifted onto Asia to overcome the singularity at the North Pole (Madec and Imbard 1996). The resolution is 92 points by 76 points, which corresponds to roughly 4º by 3º degree, with a meridional resolution of 1º near the equator. The model has 30 vertical levels, with 10 levels in the upper 100 meters. The turbulent diffusion is isopycnal-diapycnal, with a limitation of the isopycnal slopes to 1% (Guilyardi et al. *1999*). The isopycnal diffusion coefficient is 2000 m^2s^{-1}, with no background horizontal diffusion.

In order to close the global hydrological cycle, the drainage basins and outflows of the 46 major rivers have been defined at the atmospheric model resolution. Corresponding river mouths have been defined on the ocean model grid. Coastal runoff is also taken into account and pours directly into the nearest coastal boxes of the ocean model.

b. Sea ice parameterization

In the previous version of the model (Braconnot et al. 1997), thereafter referenced as DI (Diagnostic sea Ice), an ocean grid-box is supposed to be frozen when the sea-surface temperature (SST) falls below the freezing point of sea-water. The heat flux from the ocean to the bottom of sea ice is prescribed as -2 Wm^{-2} in the Northern Hemisphere (Arctic) and as -4 Wm^{-2} in the Southern Hemisphere (Antarctic) (Maykut and Untersteiner 1971). When this happens, the sea surface temperature can ony warm up by heat advection and diffusion. Since the grid resolution is greater in the ocean model than in the atmosphere, the area covered by sea ice represents a fraction in an atmospheric grid box. The surface temperature and albedo of the sea ice fraction are computed using a simple one-layer thermodynamic model and making the assumption that sea-ice is 3m-thick. At the bottom of sea-ice, the temperature is prescribed as 271,2K.

The new sea ice model developed at Laboratoire d'Océanographie Dynamique et de Climatologie (LODYC) (L'Heveder 1999), thereafter referenced as MI (Modeled sea Ice), has now been introduced in the model. At present, this model provides a complex representation of sea ice thermodynamics, but sea ice dynamical processes are still under development. It is entirely integrated into the first level of the ocean model OPA (surface layer between 0 and 10 m depth), and uses the same grid and time step..

The thermodynamic scheme is derived from the works of Hibler (1980). The model uses a realistic distribution function associated to four different ice types: open water (nil ice thickness), thin ice (thickness between 0 and 0.5 m), intermediate ice (thickness between 0.5 and 3 m), and thick ice (thickness greater than 3 m). Each ice type has its own thermodynamic behavior. For example, thin ice grows and decays more rapidly than thick ice. A variable fraction of leads in the sea ice cover is simulated in order to parameterized the open water due to ice motion at subgrid scale. The minimum lead fraction linearly decreases with ice thickness from 15% for ice thinner than 0.1 m. to 2% for ice thicker than 0.4 m. in the southern hemisphere and 1m in the northern hemisphere. The ice thermodynamic is resolved into 3 layers (one for the snow and the two others for the ice) following (Semtner 1976). A linear equilibrium temperature profile is assumed in each layer, and the vertical conduction of heat is proportional to the temperature gradient. The bottom temperature of the ice corresponds to the seawater freezing point (~ -1.8^{o}C). Temperatures at the snow-ice interface and into the ice are computed assuming flux continuity between the layers. The surface temperature T_s is determined from the surface energy balance. The surface temperature is fixed at 0^{o}C

when it exceeds the melting point and the surface energy balance is recomputed. The energy excess is then used to compute the surface melting rate of snow or ice.

The energy absorbed in the open water areas (leads) is used to melt sea ice at its bottom. A lateral ice growth can occur in leads. When ice thickening increases the ice volume, a fraction of open water is converted into thin ice. Snow accumulation on top of the ice is represented as well as its transformation into "white ice" due to snow flooding. The snow surface albedo evolves with the snow age like in the DI case. Frozen and melting ice have also their own albedo. At the bottom of the ice, the thickness can change by freezing or melting following the bottom energy balance. The evolution of an internal latent energy reservoir is resolved. It represents the internal brine pockets created by the penetration of solar radiation into the ice. Part of this radiation can also reach the ocean through sufficiently thin ice.

c. Coupling procedure

The ocean and atmosphere models are coupled synchronously once a day using the OASIS coupler developed at CERFACS (Terray 1994). No flux correction techniques are used at the air-sea interface. The atmosphere uses as surface boundary conditions the daily sea surface temperature and sea ice cover provided by the ocean. The ocean is forced by the net heat fluxes (solar and non-solar), the water fluxes (precipitation, evaporation, coastal runoff and river's flows) and the wind stresses given by the atmosphere. The surface fluxes, which are computed separately over the sea ice and free ocean fractions in the atmosphere model, are averaged over the two sub-surfaces prior to coupling.

In the classical daily coupling scheme between ocean and atmosphere, the ocean model uses a constant heat forcing during one day. Because of the characteristics (heat capacity, minimum thickness) of the sea ice, the sea ice model is unstable when it is directly forced by mean daily heat fluxes. A term of feedback between the simulated surface temperature and the heat flux is required to stabilize the system at each time step. Therefore, we use a coupling technique that allows the heat flux to vary as a function of the local surface temperature (Dufresne and Grandpeix 1996). In an ocean grid box, the non-solar heat flux over the fraction of each ice type is linearized at the first order around the mean temperature of the grid box. Therefore, the sensitivity (derivative) of the flux to the surface temperature, which is computed as the sum of the sensitivity for the turbulent heat fluxes and the infrared flux, is also provided to the ocean model. Its annual mean is smaller than -20 $Wm^{-2}K^{-1}$ in high latitudes, especially in the sea ice region (-10 $Wm^{-2}K^{-1}$). The solar radiation is also distributed according to the local albedo of each ice type.

3. Simulations

a. Initialization and spin-up

In the following, we consider a 120-years long simulation with this coupled model (MI). The initial condition of the coupled integration corresponds to January 1st of year 16 of an atmosphere alone simulation forced with the mean seasonal cycle of climatological SST (Reynolds 1988) and sea-ice cover. It is exactly the same state as the one used before for the simulation with the diagnostic sea-ice (DI) (Braconnot et al. 2000).

The ocean starts from rest and its thermohaline structure is prescribed from the climatology of Levitus (1982). The initial sea ice cover is diagnostic and corresponds to

the ocean-grid points where the SST is below the seawater freezing point. The ice concentration is fixed to 70 % and the mean thickness respectively to 1 and 3 meters in the Antarctic and in the Arctic. The spin up of the ocean-ice model is done directly with the coupled model. During the first nine years, the thermohaline structure of the ocean is restored both at surface and at depth towards the initial climatology, except under sea ice. After year nine, the coupled model can evolve freely without any flux correction or restoring. This initialization technique minimizes the coupling shock and is now used by several groups (Stouffer and Dixon 1997).

After the spin-up period the model adjusts within 10 years and the simulation is quite stable from year 20, as illustrated by the annual mean evolution of the global mean SST (Fig. 1). In absence of flux correction, this stability results from the balance of the heat fluxes at the ocean surface. The small drift is limited to 0.3 ^{o}C per century for the global SST and is less than 0.05 ^{o}C per century for the global ocean temperature. This version of the model is slightly colder than the previous one (Fig. 1), which is due to the more realistic sea-ice cover in the Arctic.

b. Sea ice cover

Indeed, after the spin up and the period of adjustment, the simulated sea ice cover is quite stable and the seasonal cycle is represented in the Northern Hemisphere (Fig. 2). Since the initial shock is absorbed after year 20, we chose the years 20 to 120 as the reference period to compute the mean seasonal cycle.

The mean seasonal cycle of the sea-ice cover in the Northern Hemisphere is realistic (Fig. 3). The maximum cover (13.7 x 10^{6}km^{2}) is similar to the mean estimate (13.5 x 10^{6}km^{2}) deduced from satellite data (Gloersen and Campbell 1991), but the minimum is too high (7.5 x 10^{6}km^{2} compared to 6 x 10^{6}km^{2} from the data). The geographical distribution of the effective sea-ice cover, excluding the open water areas included in the ice pack, is also consistent with the sea ice cover used as boundary conditions for AMIP1 simulations (Boer 1992; Gates 1992) and interpolated on the atmospheric grid (Fig. 4). However, the marginal sea ice front delimiting the maximum extension is too zonal around 65^{o}N (Fig. 4b). This is mainly due to the absence of a correct North Atlantic Drift (see section 5), which does not bring enough warmer and saltier water from mid-latitudes to the Norwegian Sea. Also, the absence of any sea ice dynamics prevents the extension of sea ice towards the Irminger Sea through the Fram and Denmark straits. Similarly, the sea ice extension is too weak in the Bering Sea.

On the other hand, the model is not able to maintain a correct sea-ice cover in the Southern Hemisphere. Part of this drawback is due to a too large solar heat flux simulated at the ocean surface. This problem is also listed in other models (Guilyardi and Madec 1997; Gordon et al. 2000). It results from a lack of low level stratus clouds all over the southern latitudes. However, it has been shown in recent simulations with the IPSL model that the seasonal runoff from Antarctica iceberg discharge has also a large contribution. (Dufresne, pers com). Sea-ice is much better simulated in the Southern Hemisphere when this fresh water flux is introduced, because it favors the formation of a halocline and in turn the freezing of seawater.

We therefore do not consider the Southern Hemisphere in this study and focus on the Northern Hemisphere where sea-ice is more realistically simulated. The correct simulation of sea-ice in the Arctic allows us to use the MI simulation to investigate the role of sea-ice in the coupled ocean-atmosphere system. It is interesting to compare the mechanisms operating in MI with those of DI. Indeed, the seasonal cycle of the sea-ice cover and other climatic parameters are also stable in DI (Fig. 1), but the sea-ice

vanishes almost entirely in September and the maximum sea-ice cover is underestimated in March (Fig. 3 and 4). There are thus important interactions between sea-ice and the circulation both in the atmosphere and in the ocean that are missing in DI and need to be considered. In the following, we investigate successively the surface heat fluxes, the fresh water fluxes and the link with the large scale surface and thermohaline circulation of the ocean.

4. Mean seasonal cycle in the Arctic: surface energy budget

In order to study in more depth the seasonal cycle of the surface heat fluxes over the Arctic Ocean, we averaged the different fields over a specific box defined according to Orvig (1970). It includes all the Arctic Ocean down to the Bering Strait for the Pacific Ocean side, and down to 65^{o}N for the Atlantic Ocean side.

From April to September the net heat flux at the surface is driven by the net solar heat flux and acts to melt the sea-ice (Fig. 5a). The non solar heat flux becomes dominant during winter (October to March) and contributes to increase the sea-ice cover. Although the annual mean surface net heat budget (-16 Wm^{-2}) is identical for the two simulations over the Arctic, the magnitude of the seasonal cycle is larger in DI (Fig. 5a.). This difference directly follows the differences in the sea-ice cover and surface temperature. There is less ice in summer in DI and the solar heat flux is 60 Wm^{-2} larger. The cooling by the non solar heat flux is also more active in November (70 Wm^{-2}) because the sea-ice cover is very poor and the mean surface temperature 20°C higher.

The behavior of sea-ice is thus very important and strongly constraints the heat budget of the Arctic. The two simulations have a comparable sea-ice cover in March (Fig. 4). However in DI, as soon as the temperature rises above the sea water freezing point (Fig. 5b), the sea ice cap disappears from the ocean grid box. Then, since the surface albedo becomes much weaker, more solar radiation can reach the surface (Fig. 5a), leading to the well-known positive direct sea ice cover-albedo feedback (Kellogg 1973; Curry et al. 1995) and thereby to the disappearance of sea ice.

Since the physical processes included in the thermodynamic model are more complex, the behavior of the sea ice in MI is not so extreme. Until May, there is still no surface melting (Fig. 5c) and the ocean temperature remains close to the freezing point (Fig. 5b). The mean sea ice concentration over the Arctic Ocean remains around 90%, and the fixed maximum of 98% is reached in the central part of the basin in May. Even if the bottom accretion decreases (Fig. 5c), it continues to thicken the ice pack that exhibits a maximum (2.3 m) of mean thickness over the Arctic in May. Then, the surface heat budget becomes positive and the surface ablation rate increases to reach a maximum of 14 mm/day during July (Fig. 5c). As shown by Fichefet and Gaspar (1988), the ocean heat flux at the bottom of the ice plays also a crucial role in the simulation of sea ice. Because of the increase of the energy supply from the ocean, sea ice melts from its bottom (Fig. 5c). Since all the energy absorbed into the leads is used under sea ice, the ocean heat flux is larger than 20 Wm^{-2} during July when the ablation rate is maximum (6.6 mm/day). This large heat absorption by the sea ice model contributes to limit the summer warming. Since the ocean temperature under sea ice is fixed to the freezing point, the mean ocean temperature over the Arctic does not exceed 0 ^{o}C, while the mean surface temperature does not exceed +0.5 ^{o}C (Fig. 5b).

In September, the mean concentration and the mean thickness over the Arctic are at their minimum (63% and 1.1 m respectively). The surface energy budget becomes negative again (Fig. 5a), the temperature goes down and the sea ice concentration increases. Since the energy lost into the leads is taken from the bottom of sea ice, the

mean thickness increases by bottom growth of the ice. Thus, both the temperature cooling and the insulator effect of sea ice limit the non solar heat fluxes, and stabilize the system (Kellogg 1973). This regulation loop via the heat fluxes allows to reconstruct each year the maximum of sea ice cover. This mechanism also operates in DI, and leads to the reconstruction of the sea ice cover during the winter.

This analysis clearly shows that the albedo feedback and the insulator effect of sea-ice are not sufficient to represent correctly the sea-ice cover of the Arctic and that the thermodynamic processes controlling the inertia of the sea-ice need to be accounted for. The resolution of the ice heat budget independently in 3 layers and the thermodynamics of leads play an important role and introduce leads and lags in the system.

Interestingly, the impact of the sea-ice parameterization on the surface temperature is limited to the Arctic basin and the Atlantic sector (Fig. 6a). There is almost no difference between the two simulations over land, except a slight cooling along the Arctic coast and in Siberia during winter only. The Arctic cooling affects the atmospheric structure up to 600 hPa, but only for latitudes higher than 60°N (Fig. 7). However, the whole thermal structure of the ocean is affected. The impact of sea-ice seems thus only local for the atmospheric circulation, as can be inferred from the change in 500 hPa geopotential height between MI and DI (Fig. 6b). On the other hand, its impact is more global for the oceanic circulation. This is investigated below.

5. Hydrology and circulation in Arctic and North Atlantic

a. Surface salinity and circulation in the north

A low salinity anomaly is built up along the Siberian coasts during the first year of both simulations. It then moves through the Barents Sea, leading to a rapid decrease of the surface salinity in the Barents Sea and in the Greenland, Iceland, Norwegian seas (GIN seas). It is due to an unrealistic anticyclonic atmospheric circulation over the Greenland Sea and the Norwegian Sea, and to a shift of the oceanic polar gyre towards the Spitzberg. The fresh waters from the great Siberian rivers are advected to the entrance of the Norwegian Sea.

However after this initial drift, the two simulations have very different adjustments. The surface salinity recovers very slowly in MI, while the anomaly intensifies slowly through time in DI –without any preferential season-. The mean vertical profiles of salinity and temperature are thus very different between the two simulations in the GIN seas. In March, a strong halocline affects the first 300 meters of the water column in DI (Fig. 8a). The gradient between the surface and the bottom reaches 2.3 PSU. The temperature profile (Fig. 8b) presents a strong inversion. The situation is thus stable and no convection can occur. In MI, the gradient between the surface and 300 meters depth is only 0.3 PSU (Fig. 8a), and the surface temperature remains near 0 °C. Surface potential density is thus sufficient to allow the sinking of surface waters. Because of convection and mixing, the temperatures of the water column are more homogenous.

The atmospheric and oceanic circulation in the North Atlantic and the GIN seas are also very different between the two simulations. In the real ocean, the North Atlantic Drift brings some sub-tropical warmer and salty waters into the Norwegian Sea and Greenland Sea (Schmitz and McCartney 1993). These waters penetrate along the coasts of Scandinavia via the Norwegian current, and a small part continues along the coasts of Siberia. In DI, the mean flow simulated at mid-latitudes is very zonal and the mean surface currents in the South of Iceland are very weak (Fig. 9a). The intensity of the sub-polar gyre is limited to about 5 Sv, with no extension into the Norwegian Sea (Fig. 9a). In MI, the meridional component of the surface currents at mid latitudes is enhanced (Fig. 9b). The sub-polar gyre is much stronger with a maximum of 18 Sv into the

Irminger Sea, and extends northward into the Norwegian Sea (Fig. 9b). Even if this extension is still too limited, a mixing between North Atlantic salty waters and Norwegian Sea fresher waters can occur.

Since we only changed the parameterization of sea-ice between DI and MI, these differences in the model behavior are the signature of different interactions between the sea-ice, the hydrological cycle and the circulation in both the atmosphere and the ocean.

b. Surface fresh water inputs into the Arctic

Changes in the fresh water inputs between the two simulations could be at the origin of the differences between the two simulations. Compared to the estimation of Aagaard and Carmack (1989), the annual mean budget of surface fresh water fluxes is under-estimated by about 20% in both simulations (Table 1) and therefore cannot explain the maintenance of the salinity anomaly in DI. This budget only includes the contribution of continental runoff and P-E (precipitation minus evaporation) since sea-ice has no impact on the fresh water fluxes in the annual mean.

River runoff is a critical source of fresh water in the Arctic (Weatherly and Walsh 1996; Miller and Russell 1997). The simulated annual mean discharges of the eight major rivers and the direct coastal runoff are similar between the two simulations and underestimated (Table 1). A comparison with the values given by a data compilation (Perry et al. 1996) shows this comes from a underestimation of the discharges of the largest rivers located in the middle of the Siberian coast (Fig. 10). In particular, there is a deficit of precipitation over the drainage basins of the Ob and Ienesseï rivers. The discharges of the smallest rivers located on the eastern part of the Siberian coast are over-estimated mainly because the size of their drainage basins are over-estimated in the coarse resolution of the atmosphere model at high latitudes.

The contribution of P-E is more different between MI and DI, since the annual fresh water input over the Arctic Ocean from P-E is +20% larger in MI (Table 1). Because of the insulating effect of sea-ice, the annual mean evaporation is reduced by almost 50% over the basin, whereas the annual mean total precipitation (rain plus snow) is reduced only by 15%. These changes follow the differences of sea-ice cover and temperature over the Arctic Ocean and so are maximum in early fall. Nevertheless, these differences are not sufficient to alter significantly the salinity of the GIN seas.

c. Impact of sea-ice on the atmospheric and oceanic circulation

The differences between MI and DI result thus mainly from differences in the oceanic and atmospheric circulation. They are induced by the sea-ice characteristics and interaction with the fresh water cycle.

The differences in the simulated sea-ice cover between MI and DI is the first factor that can explain the different oceanic circulation described above. In both simulations, the Icelandic low-pressure zone is shifted to the West. This shift already exists in the atmosphere alone simulation as in many models (Kageyama et al. 1999), but is reinforced in the coupled simulations (Laurent et al. 1998). The tail of the storm-tracks does not extend far enough across the North Atlantic towards Europe, and easterlies dominate the simulated circulation instead of southwesterlies over the south of Iceland. However, the more realistic sea-ice cover simulated in MI during fall and winter leads to colder temperature in the Arctic (Fig. 6), and in turn higher surface pressure than in DI. The pressure gradient between the Icelandic low and the Arctic is enhanced and more realistically represented (Fig. 9c). Compared to DI, the surface winds are strengthened in

this region (Fig. 9c), inducing a larger northward Ekman transport, and thereby a surface import of warmer and saltier waters from the Atlantic into the Arctic. The transport of water mass through the Iceland-Faeroe-Scotland ridge reaches 4.7 Sv in annual mean (against 0.7 Sv in DI) and prevents the development of the initial salinity anomaly.

The second effect of sea- ice involves a complex loop between the impact of sea-ice on the hydrological cycle (salinity), the characteristics of water masses in the GIN seas and deep convection. Indeed sea ice has a crucial role on the surface salinity at the seasonal time scale, through the processes of brine rejection during its formation, and fresh water release during its melting. At high latitudes, these processes could have a direct impact on the rate and location of deep convection and bottom water formation (Lenderink and Haarsma 1996). In the GIN seas area, the mean surface salinity is higher throughout the year in MI (Fig. 11a). In addition, brine rejection and fresh water release due to the seasonal cycle of sea ice, which are not considered in DI, introduce a seasonal variability of the surface salinity. The winter surface salinity is 1 PSU larger than the summer value. Combined with the winter cooling of the sea surface temperature, this higher salinity enhances the sea surface potential density and thus destabilizes the water column. This vertical mixing in MI (Fig. 11b) is also well illustrated by the difference of the zonally global averaged ocean temperatures between the two simulations (Fig. 7). Between 60^{o}N and 80^{o}N, the first 500 meters are colder in MI, whereas the waters below are warmer especially around 1500 m. In turn the convection strengthens the surface water advection. These results illustrate the strong coupling between sea-ice, the surface and the thermohaline circulation.

6. Impact on the thermohaline circulation and the equator-to pole heat transport

The annual mean integrated export through the Greenland-Iceland ridge reaches 6.1 Sv in MI (1.6 SV for DI), with a maximum at the bottom. The heat is exported at depth in the North Atlantic, as the first part of the thermohaline conveyor belt (Gordon 1986). In our model, the other source of deep water winter convection is centered south of Iceland at about 55^{o}N, whereas it should be located in the Irminger and Labrador seas. The position of this convection zone in the model is not well understood. It is a common feature of many ocean circulation model (Manabe and Stouffer 1994), and is already present in ocean alone simulation forced by surface heat and fresh water fluxes climatology (Esbensen and Kushnir 1981; Oberhüber 1988). The convection in this region does not change between the two simulations.

The formation of dense water in the Norwegian Sea plays thus an important role in the annual mean overturning stream function (Fig. 12). The surface waters sink around 60^{o}N until the bottom ridge down to 2000 m, while in DI the sinking signal is diffuse and affects only intermediate depths down to 1000 m. The annual mean maximum of the overturning function in North Atlantic (between 500 and 5000 meters, and between 10^{o}N and 70^{o}N) can be considered as an index of the strength of the thermohaline circulation. This mean index is only 9.1 Sv in DI, whereas it reaches about 14.6 Sv in MI. Therefore, the upwelling at the equator is stronger in MI and the thermocline is narrower and exhibits a well-simulated "W"-structure (Fig. 7). Between 30^{o}S and 30^{o}N, the intermediate waters around 500 meters are cooler. Nevertheless, the intensity of the North Atlantic Deep Water (thereafter NADW) is still too weak according to estimates (Schmitz and McCartney 1993).

These differences in the thermohaline circulation have a large impact on the equator to pole oceanic heat transport. The poleward heat transport by the Atlantic Ocean is nearly doubled in MI compared to DI (Fig. 13a). At 35^{o}N latitude, its maximum is about

0.6 PW in MI and only 0.3 PW in DI. The Atlantic heat transport in MI is not only closer to the estimations of Trenberth and Salomon (1994) -which gives peak values of 1.1±0.2 PW at 20 to 30^{o}N in the Atlantic-, but is also now positive (northward) at all latitude in both hemispheres. Differences in the total atmospheric heat transport between the two simulations are limited to the higher latitudes (beyond 40^{o}N) (Fig. 13b). North of 30^{o}S, differences in the heat transport by the global ocean are entirely dominated by the changes in the Atlantic basin. Finally, the total heat transport is enhanced by 0.2 PW in MI for latitudes located between 30^{o}S and 30^{o}N. The maximum value 0.8 PW reached at 35^{o}N is closer to the observed estimate.

7. Conclusion

The sensitivity of the IPSL coupled ocean-atmosphere model to a change in sea-ice parameterization illustrates well the important interactions between sea-ice and both the oceanic and atmospheric circulation at high northern latitudes. Our results are based on the comparison of a simulation, which includes a complex thermodynamic sea-ice model (MI), and a simulation with the previous version of the model where sea-ice was only diagnostic in the ocean (DI). These two coupled simulations have been performed without flux correction at the air-sea interface and differ only by the sea ice parameterization used. The sea-ice model used for MI is more sophisticated than the thermodynamic parameterizations included in most of the coupled models referenced in the CMIP project. In particular, it includes several ice-types computing a fraction of leads, and it resolves the thermodynamic of sea-ice in three layers taking account of an internal latent heat reserve.

The sea-ice albedo feedback and the insulator effect of sea-ice are sufficient to produce a stable simulation of the Arctic climate in DI, with an annual reconstruction of the sea-ice cover. Nevertheless, they do no allow for a good representation of the seasonal cycle neither of the sea-ice characteristics and nor of the circulation over the Arctic and the North Atlantic. Our study confirms that the thermal inertia of sea-ice plays a crucial role in regulating the sea-ice cover, the sea-ice thickness, and thereby the mean surface temperature and the seasonal cycle of the surface heat fluxes in the Arctic. It shows that it is important to resolve the heat budget for the ice independently at the interfaces between the atmosphere and the ocean, and also within the ice. Indeed, the seasonal cycle of these fluxes is not in phase, and time lags between them increase the sea-ice inertia.

A realistic seasonal evolution of the sea-ice cover is needed to properly simulate the surface temperature over the Arctic. The impact of sea-ice on the atmospheric circulation however, is limited to the Arctic and North Atlantic. There is nearly no change over land where precipitation is underestimated in both simulations, which leads to an underestimation of the river runoff in the Arctic.

The impact of sea-ice and of the coupling between the sea-ice cover and the atmospheric circulation has an important effect on the oceanic circulation. The thermal structure of the ocean is altered both in the North Atlantic and in the tropical regions where the shape of the thermocline is very sensitive to small changes in ocean upwelling. These large differences between the two simulations result mainly from what happens in the Norwegian Sea. When the sea-ice cover simulated is coherent with the observations, the pressure gradient between the high surface pressure located over the Arctic and the Icelandic low induces southwesterly wind around Iceland. The associated Ekman transport favors the penetration into the Norwegian Sea of the North Atlantic Drift. The import of saline and relatively warm waters together with the seasonal cycle

induced by ice brine rejection and sea-ice melting favor the deep water convection in winter, and the formation of deep waters. These waters are exported at depth through the Denmark Strait as a branch of the thermohaline circulation.

The coupling between a more active transport in the west boundary current, the north Atlantic Drift and the convection in the Norwegian sea is also very important to simulate a correct Atlantic equator to pole ocean heat transport. The only introduction of a more complex thermodynamic sea-ice model increases the ocean heat transport from 0.3 to 0.6 PW in the Atlantic at 35^{o}N. The whole thermohaline structure of the Atlantic Ocean is improved.

Acknowledgements We would like to thank the LODYC for providing the ocean and sea ice models, the LMD for the atmosphere model, and the CERFACS for the coupler OASIS and the VAIRMER software for handling and post-processing the model outputs. The computer time was provided by the Commissariat à l'Energie Atomique. Y.L. thanks the Commissariat à l'Energie Atomique for PhD scholarship support during the course of this work.

References

Aagaard K., L. K. Coachman, and E. C. Carmack, 1981: On the halocline of the Arctic Ocean. *Deep-Sea Research*, **28**, 529-545.

Aagaard K., and E. C. Carmack, 1989: The role of sea ice and other fresh water in the Arctic circulation. *Journal of Geophysical Research*, **94**, 14.485-14.498.

Andrich P., P. Delecluse, C. Levy, and G. Madec, 1988: A multitasked general circulation model of the ocean. *Proc. Fourth Int. Symp. on Science and Engineering on Cray Supercomputers*, Minneapolis, Minnesota, Cray Inc., 407-428.

Boer G. J., 1992: Some results from and an intercomparison of the climates simulated by 14 atmospheric general circulation models. *J.Geophys. Res*, **97**, 12.771-12.786.

Braconnot P., O. Marti, and S. Joussaume, 1997: Adjustements and feedbacks in a global coupled ocean-atmosphere model. *Climate Dynamics*, **13**, 507-519.

Braconnot P., S. Joussaume, O. Marti, and N. de Noblet, 1999: Synergistic feedbacks from ocean and vegetation on the African monsoon response to mid-Holocene insolation. *Geophysical Research Letters*, **26**, 2481-2484.

Braconnot P., O. Marti, S. Joussaume, and Y. Le Clainche, 2000: Ocean feedback in response to 6kyr BP insolation. *Journal of Climate*, **13**, 1537-1553.

Cubash U., K. Hasselmann, H. Hock, E. Maier-Reimer, U. Mikolajewicz et al., 1992: Time-dependent greenhouse warming computations with a coupled ocean-atmosphere model. *Climate Dynamics*, **8**, 55-69.

Curry J. A., J. L. Schramm, and E. E. Ebert, 1995: Sea Ice-Albedo Climate Feedback Mechanism. *Journal of Climate*, **8**, 240-247.

Delecluse P., G. Madec, M. Imbard, and C. Levy, 1993: OPA version 7 general circulation model reference manual. Laboratoire d'Océanographie Dynamique et de Climatologie Internal Report, 102 pp. [Available from LODYC, 4 place Jussieu, boite 100, F-75252 PARIS Cedex 05, France.]

Dufresne J.-L., and J.-Y. Grandpeix, 1996: Raccordement des modèles thermodynamiques de glace, d'océan et d'atmosphère. Laboratoire de Modélisation Dynamique Note Interne 205, 24 pp. [Available from LMD, 4 place Jussieu, boite 99, F-75252 PARIS Cedex 05, France.]

ECMWF, 1992: Research manual 3, ECMWF Forecast model, physical prametrization.

Esbensen S. K., and V. Kushnir, 1981: The heat budget of the Global Ocean : an atlas based on estimates from marine surface observations. Climatic Research Institution, Oregon Sate University Rep. 29

Fichefet T., and P. Gaspar, 1988: A model study of upper ocean-sea ice interaction. *Journal of Physical Oceanography*, **18**, 181-195.

Gates W. L., 1992: AMIP. *Bulletion of American Meteorological Sociey*, **73**, 1962-1970.

Gloersen P., and W. J. Campbell, 1991: Recent variations in Arctic and Antarctic sea-ice covers. *Nature*, **352**, 33-36.

Gordon A. L., 1986: Interocean exchange of thermohaline. *Journal of Geophysical Research*, **91**, 5037-

5046.

Gordon C., C. Cooper, C. A. Senior, H. Banks, J. M. Gregory et al., 2000: The simulation of STT, sea ice extends and ocean heat transports in a version of the hadley centre coupled model without flux adjustments. *Climate Dynamics*, **16**, 147-168.

Guilyardi E., and G. Madec, 1997: Performance of the OPA/ARPEGE-T21 global ocean-atmosphere coupled model. *Climate Dynamics*, **13**, 149-165.

Guilyardi E., G. Madec, and L. Terray, 1999: The role of lateral ocean physics in the upper ocean thermal balance of a coupled oean-atmosphere model. Institut Pierre Simon Laplace Note 13, 19 pp. [Available online at http://www.ipsl.jussieu.fr/modelisation/liste-notes.html]

Harzallah A., and R. Sadourny, 1995: Internal versus SST forced atmospheric variability as simulated by an atmospheric general circulation model. *Journal of Climate*, **8**, 474-498.

Hellerman S., and M. Rosenstein, 1983: Normal monthly wind stress over the world ocean with error estimates. *Journal of Physical Oceanography*, **13**, 1093-1104.

Hibler W. D. I., 1980: Modeling a variable thickness sea ice cover. *Monthly Weather Review*, **108**, 1943-1973.

Houghton J. T., L. G. Meira Filho, B. A. Callander, N. Harris, A. Kattenberg et al., Eds., 1996: Climate Change: The 1995 IPCC Assessment. Cambridge University Press, 572 pp.

Johns T. C., R. E. Carnell, J. F. Crossley, J. M. Gregory, J. F. B. Mitchell et al., 1997: The second Hadley Center coupled ocean-atmosphere GCM : model description, spinup and validation. *Climate Dynamics*, **13**, 103-134.

Kageyama M., P. J. Valdes, G. Ramstein, C. Hewitt, and U. Wyputta, 1999: Northern Hemisphere storm tracks in present day and last glacial maximum climate simulations : a comparison of the European PMIP models. *Journal of Climate*, **12**, 742-760.

Kellogg W. W., 1973: Climate feedback mechanisms involving the polar regions. *Climate of the Arctic*, Weller G., and S. A. Bowling, Eds., Geophysical Institute, 111-116.

L'Heveder B., 1999: Variabilité saisonnière et interannuelle des glaces de mer en Arctique : influence des interactions avec l'atmosphère. Université Paris VI, Thèse de Doctorat Océanologie, Météorologie et Environnement

Laurent C., H. Le Treut, Z.-X. Li, L. Fairhead, and J.-L. Dufresne, 1998: The influence of resolution in simulating inter-annual and inter-decadal variability in a coupled ocean-atmosphere GCM, with emphasis overf the North Atlantic. Institut Pierre Simon Laplace Note 8, 38 pp. [Available online at http://www.ipsl.jussieu.fr/modelisation/liste-notes.html]

Lenderink G., and R. J. Haarsma, 1996: Modeling convective transitions in the presence of sea ice. *Journal of Physical Oceanography*, **26**, 1448-1467.

Levitus S., 1982: Climatological Atlas of the world ocean. National Oceanic and Atmospheric Administration NOAA Professional Paper 13, 173 pp.

Lunkeit F., R. Sausen, and J. M. Oberhuber, 1996: Climate simulations with the global atmosphere-ocean model ECHAM2/OPYC, Part I : present-day climate and ENSO events. *Climate Dynamics*, **12**, 195-212.

Madec G., and M. Imbard, 1996: A global ocean mesh to overcome the North Pole singularity. *Climate Dynamic*, **12**, 382-388.

Manabe S., and R. J. Stouffer, 1994: Multiple-century response of a coupled ocean-atmosphere model to an increase of atmospheric CO_2. *Journal of Climate*, **7**, 5-23.

Maykut G. A., and N. Untersteiner, 1971: Some results from a time dependent thermodynamic model of sea ice. *Journal of Geophysical Research*, **76**, 1550-1575.

Miller J. R., and G. L. Russell, 1997: Investigating the interactions among river flow, salinity and sea ice using a global coupled atmosphere-ocean-ice model. *Annals of Glaciology*, **25**, 121-126.

Moore A. M., and H. B. Gordon, 1994: An investigation of climate drift in a coupled atmosphere-ocean-sea ice model. *Climate Dynamics*, **10**, 81-95.

Murphy J. M., 1994: Transcient responses of the Hadley Center coupled ocean-atmosphere model to increasing carbon dioxide, Part I : Control climate and flux adjustment. *Journal of Climate*, **8**, 36-56.

Oberhüber J. M., 1988: An atlas based on the COADS data set: the budget of heat, buoyancy and turbulent kinetic energy at the surface of the global ocean. Max-Planck-Institut für Meteorologie Report 15, 42 pp. [Available from Mac-Planck-Institut für Meteorologie, Bundestrasse 55, D-20146 Hamburg, Germany.]

Orvig S., 1970: Climates of the Polar Regions. Elsevier, 370 pp.

Perry G. D., P. B. Duffy, and N. L. Miller, 1996: An extended data set of river discharges for validation of general circulation models. *Journal of Geophysical Research*, **101**, 21.339-21.349.

Reynolds R. W., 1988: A real-time global sea surface temperature analysis. *Journal of Climate*, **1**, 75-86.

Rind D., R. Healy, C. Parkinson, and C. Martinson, 1995: The role of sea ice in $2xCO_2$ climate model sensitivity. Part I: the total influence of sea ice thickness and extend. *Journal of Climate*, **8**, 449-463.

Royer J.-F., S. Planton, and M. Dequé, 1990: A sensitivity experiment for the removal Arctic sea ice with the french spectral general circulation model. *Climate Dynamics*, **5**, 1-17.

Sadourny R., and K. Laval, 1984: January and July performances of the LMD general circulation model. *New perspective in climate modeling*, Berger A., and C. Nicolis, Eds., Elsevier, 173-198.

Schmitz W. J. J., and M. S. McCartney, 1993: On the North Atlantic circulation. *Reviews od Geophysics*, **31**, 29-49.

Semtner A. J. J., 1976: A model for the thermodynamic growth of sea ice in numerical investigations of climate. *Journal of Physical Oceanography*, **6**, 379-389.

Semtner A. J. J., 1987: A numerical study of sea ice and ocean circulation in the Arctic. *Journal of Physical Oceanography*, **17**, 1077-1099.

Smith S. D., R. D. Muench, and C. H. Pease, 1990: Polynyas and leads : an overview of physical processes and environnement. *Journal of Physical Research*, **95**, 9461-9479.

Stouffer R. J., and K. W. Dixon, 1997: Initialization of coupled models for use in climate studies : a review. CLIVAR Working Group on Coupled Modelling Report of the First Session, Appendix D [Available online at http://www.clivar.org/publications.html#clipubs]

Terray L., 1994: The OASIS coupled user guide version 1.0. CERFACS Technical Report CMGC/94-33, pp.

Trenberth K. E., and A. Salomon, 1994: The global heat balance: heat transports in the atmosphere and ocean. Climate Dynamics, 10, 107-134.

Van Ypersele J.-P., 1990: Modelling sea ice for climate studies. *Climate-ocean interaction*, Schlesinger, Eds., Kluwer Academy, 97-123.

Vavrus S. J., 1999: The response of the coupled Arctic sea ice-atmosphere system to orbital forcing and ice motion at 6kyr and 115 kyr BP. *Journal of Climate*, **12**, 873-896.

Washington W. M., and G. A. Meehl, 1996: High-latitude climate change in a global coupled ocean-atmosphere-sea ice model with increased atmospheric CO_2. *Journal of Geophysical Research*, **101**, 12.795-12.801.

Weatherly J. W., and J. E. Walsh, 1996: The effects of precipitation and river runoff in a coupled ice-ocean model of the Arctic. *Climate Dynamics*, **12**, 785-798.

Weatherly J. W., B. P. Briegleb, and W. G. Large, 1998: Sea ice and polar climate in the NCAR CSM. *Journal of Climate*, **11**, 1472-1486.

Table 1: Simplified annual mean balance (years 20 to 120) of the surface fresh water inputs in the Arctic basin (both in mm/day and km^3/year) as estimated from DI and MI, and from data by (Aagaard and Carmack 1989). The P-E budget and the total runoff are presented separately, and then cumulated in the total.

	DI Experiment		MI Experiment		Estimation	
Area	$11.634\ 10^6$ km^2		$11.634\ 10^6$ km^2		$12.10\ 10^6$ km^2	
Unit	mm/day	km3/year	mm/day	km3/year	mm/day	km3/year
P-E Budget	0.434	1818	0.521	2182	0.388	1690
Runoff	0.497	2082	0.463	1939	0.854	3720
Total	0.931	3899	0.984	4121	1.242	5410

Figure captions

FIG. 1. Time series of the annual global mean sea surface temperature (^{o}C) from year 1 to year 120 for MI *(solid line)*. For comparison, we have reported the same curve obtained for DI *(dotted line)* (see Braconnot et al. 2000 for a complete description). The different behavior between MI and DI during the first ten years is due to different spin up technics.

FIG. 2. Time series of monthly mean effective sea ice cover (10^6 km^2) in the Northern Hemisphere from year 1 to year 120 for MI.

FIG. 3. Mean monthly seasonal cycle of the effective sea ice cover (10^6 km^2) in the Northern Hemisphere for MI *(solid line)*, for DI *(dotted line)* and for the climatological data used in AMIP1 *(dashed line)*. The extrema of sea ice extension estimated from satellite data (Gloersen et al. 1991) are also plotted *(Min. and Max. dashed lines).*

FIG. 4. Mean March *(left)* and September *(right)* sea ice concentration (%) **(a)** for the climatological data used in AMIP1, **(b)** for MI and **(c)** for DI (The contour interval is 10% and values greater than 15% are *shaded*).

FIG. 5. Mean monthly seasonal cycles over the Arctic ocean of **(a)** the net surface heat fluxes (Solar, Non Solar and Total) (W.m^{-2}) and **(b)** the surface temperatures (Ocean and Mean Surface) (^{o}C) for MI *(solid curves)* and for DI *(dotted curves)*, and of **(c)** the sea ice budget (mm/day) for MI: bottom growth rate *(solid line)*, surface snow or sea ice ablation rate *(dashed line)*, and snow accumulation *(dotted line)*.

FIG. 6. Differences of MI minus DI **(a)** annual mean surface temperature (^{o}C) (The contour interval is 1°C. Values greater than 1°C are in *heavy gray* and values smaller than -1°C are in *light gray*) and **(b)** 500 hPa geopotential height (m) (The contour interval is 5 m and positive values differences are *shaded*) over the northern hemisphere (beyond 30^{o}N).

FIG. 7. Differences MI minus DI annual zonal mean temperature (^{o}C) for the atmosphere *(top)* and the ocean *(bottom)* respectively plotted as a function of altitude and depth (The contour interval is 0.25^{o}C and positive values differences are *shaded*). The first 1000 meters of the ocean are expanded.

FIG. 8. Mean March vertical profiles of **(a)** salinity (PSU) and **(b)** temperature (^{o}C) plotted as a function of depth for MI *(solid line)* and for DI *(dashed line)* at point (70^{o}N, 10^{o}W) located in the Norwegian Sea.

FIG. 9. Annual mean barotropic stream function (Sv) (The contour interval is 1 Sv and negative values are *shaded*) and surface currents (m.s^{-1}) (The vector upper right of the panel **(a)** gives the scale for a surface current of 0.1 m.s^{-1}) for **(a)** DI and **(b)** MI. **(c)** Differences MI minus DI annual mean sea level pressure (hPa) (The contour interval is 0.25 hPa and negative values differences are *shaded*) and surface wind stress (Pa) (The vector upper right of the panel **(c)** gives the scale for a surface wind of 0.1 Pa).

FIG. 10. Annual mean flows (km^3/year) of the major rivers pouring into the Arctic basin estimated from data (Perry et al. 1996) (*black*), and simulated by MI (*light gray*) and DI (*white*).

Fig. 11. Mean monthly seasonal cycle over the Greenland, Iceland and Norwegian seas (GIN seas) of **(a)** the surface salinity (PSU) and **(b)** the mixed layer depth (m) for MI *(solid lines)* and for DI *(dashed lines).*

FIG. 12. Annual mean global overturning stream function (Sv) for (a) MI and (b) DI (contour interval is 2 Sv and negative values are *dashed*), and for (c) the difference MI-DI (contour interval is 0.5 Sv and negative values are dashed and shaded). The first 1000 meters of the ocean are expanded.

Fig. 13. (a) Annual zonal mean poleward heat transport (PW) by the Atlantic Ocean as a function of latitude for MI *(solid lines)* and for DI *(dashed lines).* **(b)** Difference MI minus DI annual zonal mean poleward heat transport (PW) as a function of latitude: contributions from the atmosphere *(dotted line)*, the Atlantic Ocean *(dashed line)* and the global Ocean *(solid line)* are shown.

Figure 1

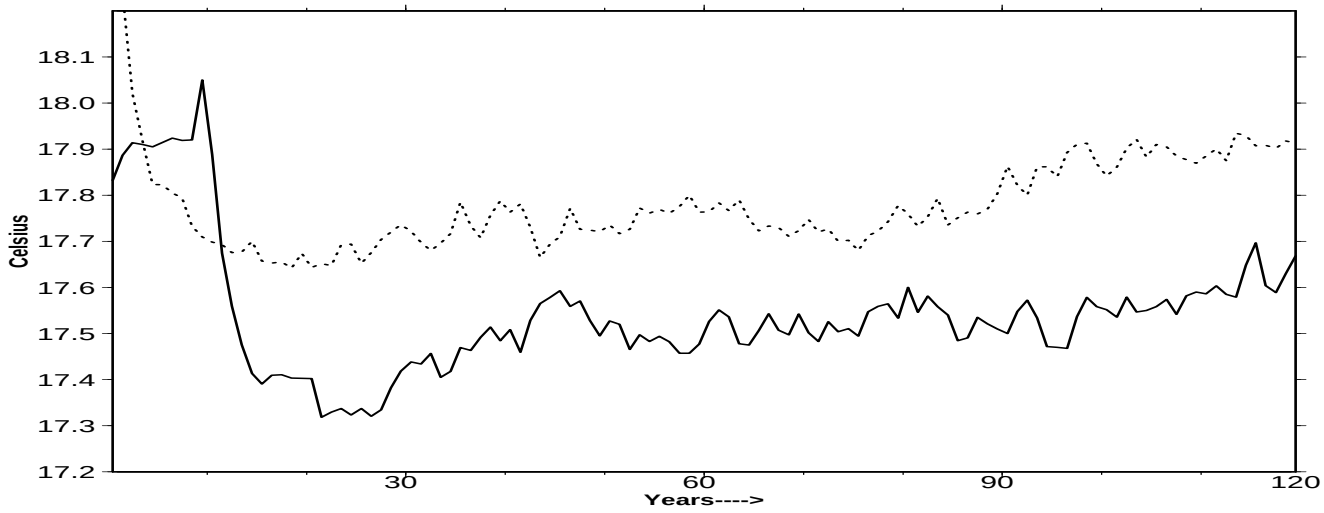

Figure 2

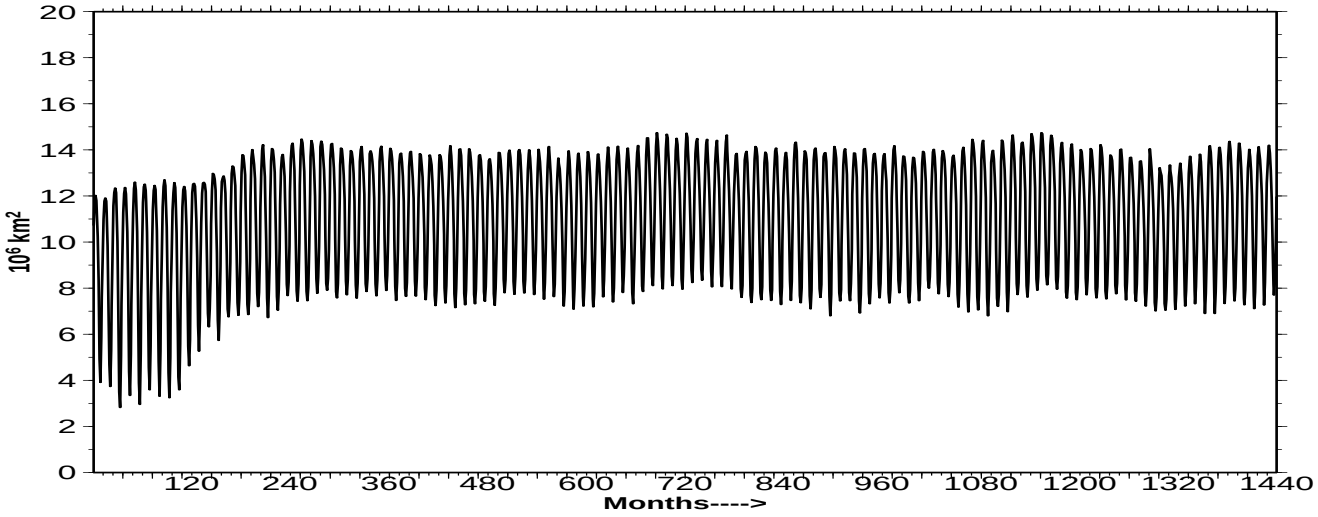

Figure 3

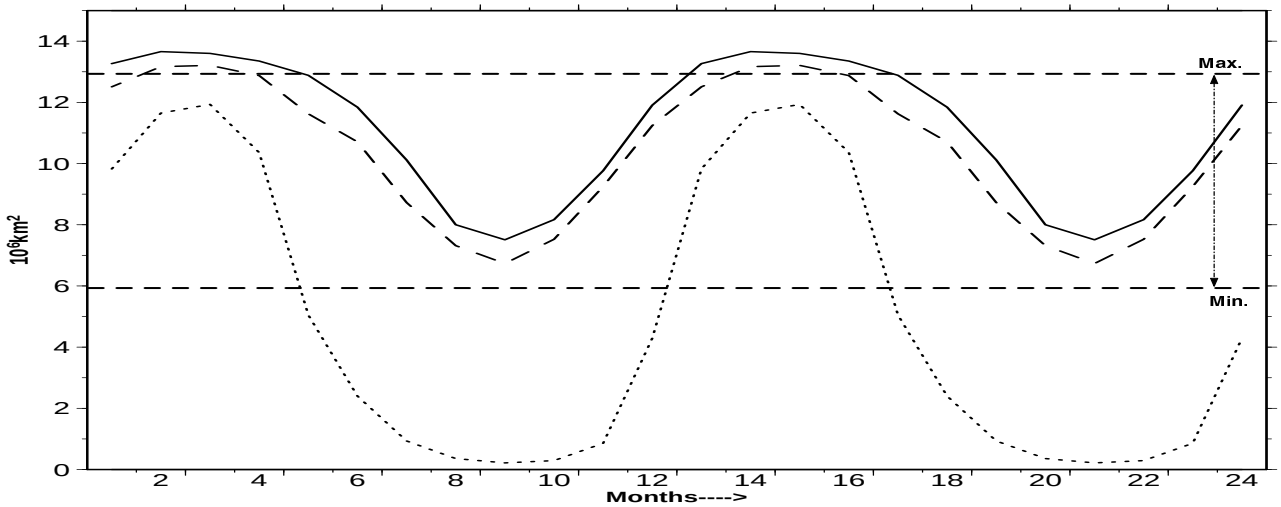

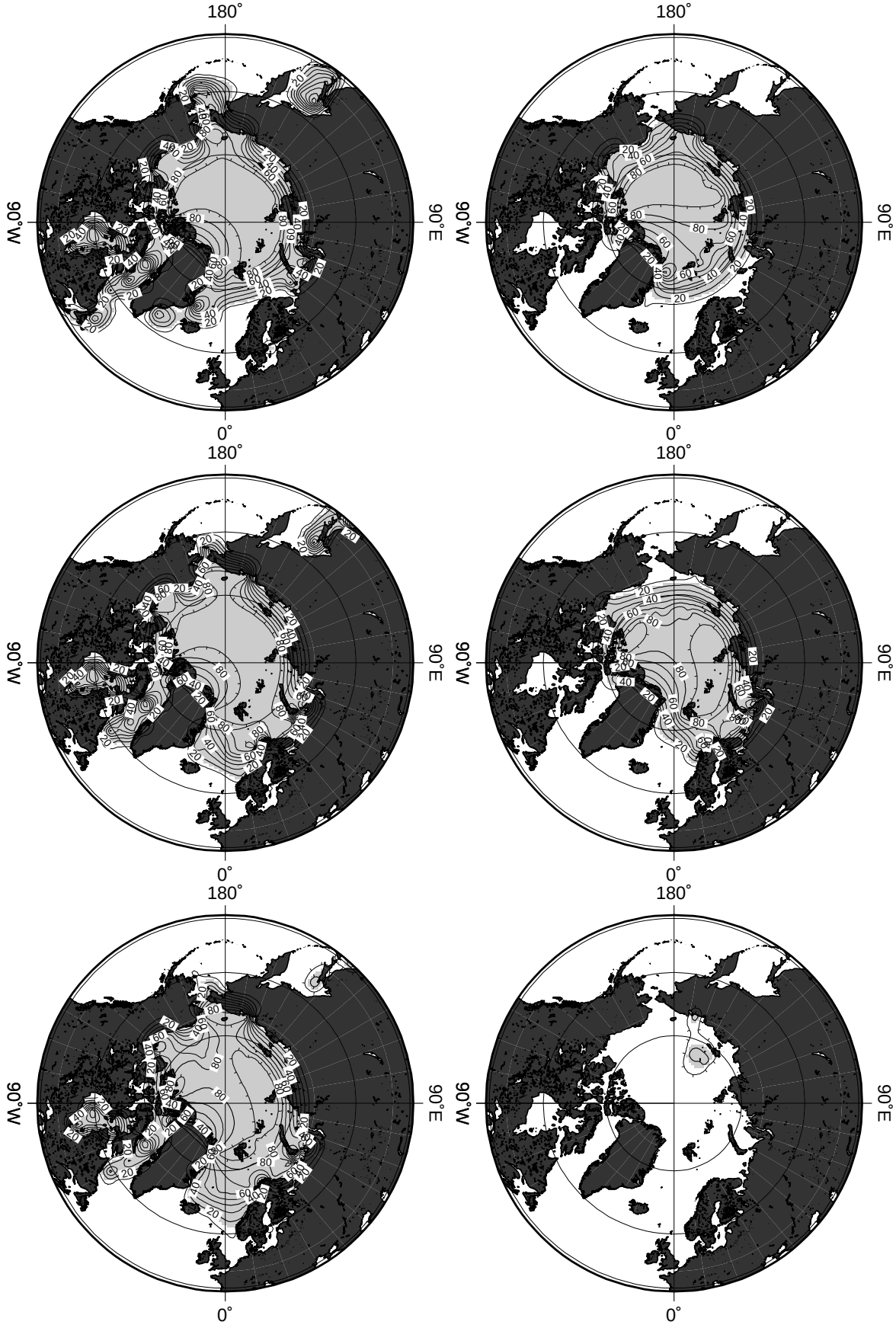

Figure 4

Figure 5

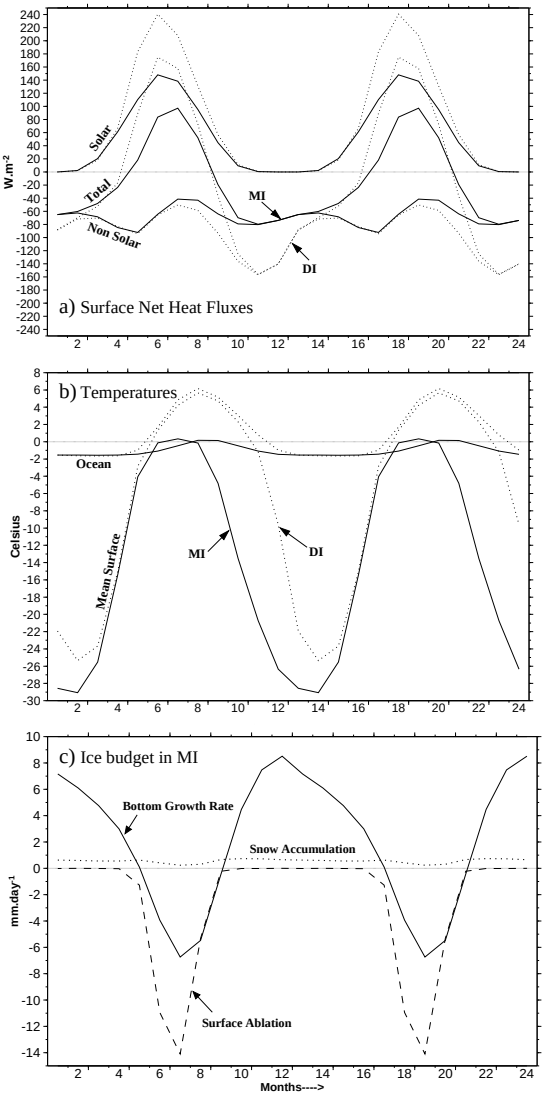

Figure 7

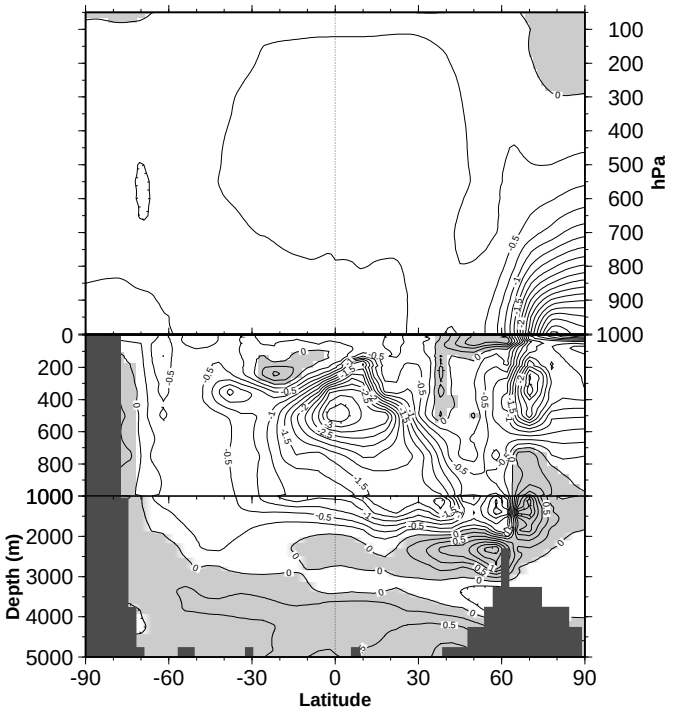

Figure 6

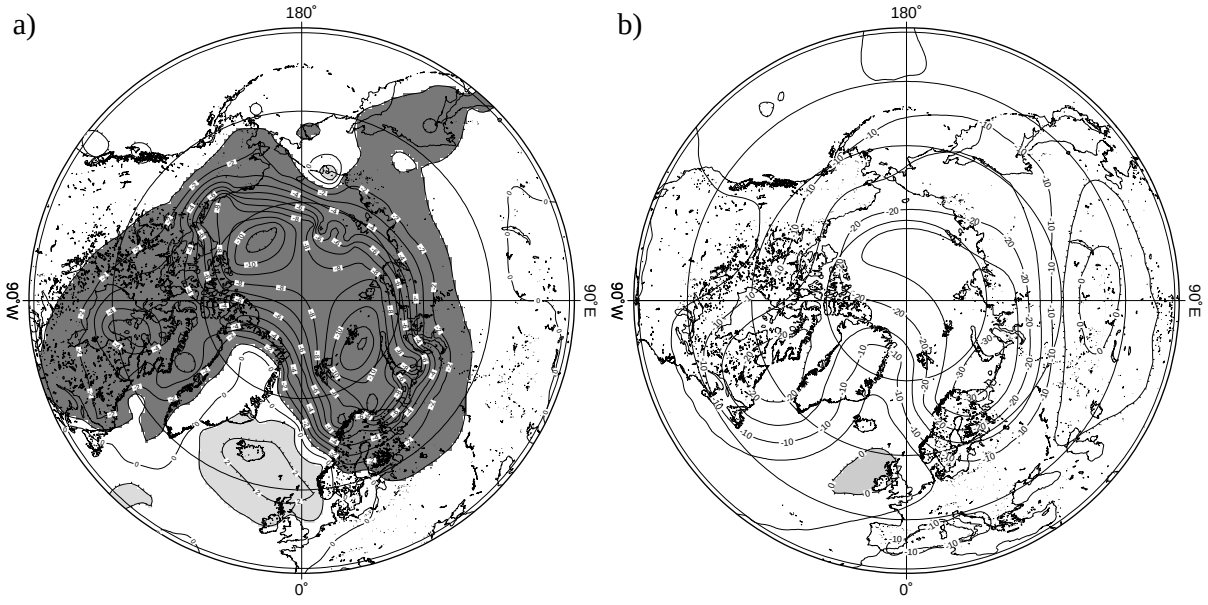

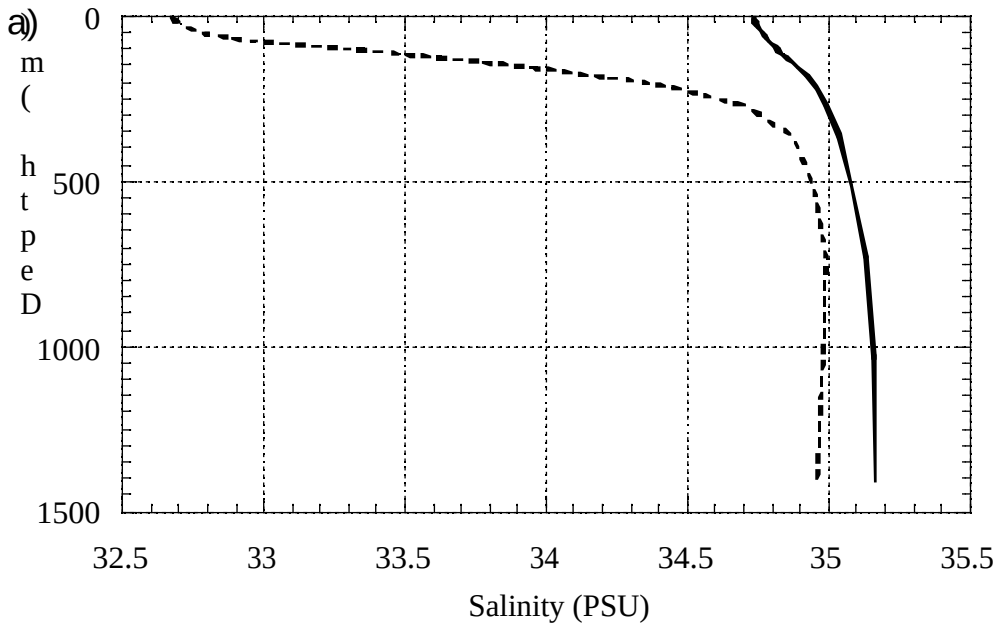
a)
Depth (m)
0
500
1000
1500
32.5
33
33.5
34
34.5
35
35.5
Salinity (PSU)

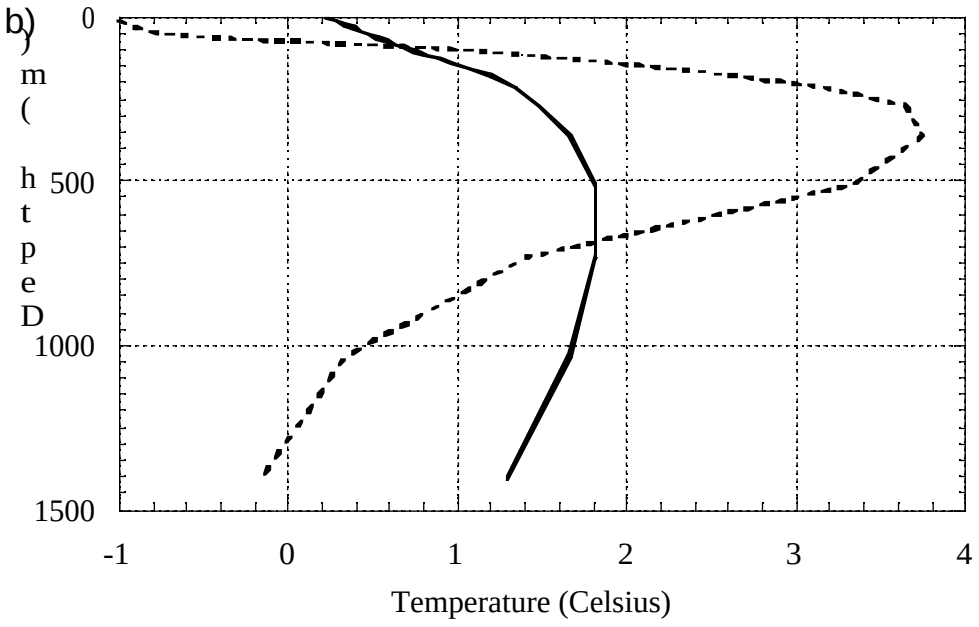
b)
Depth (m)
0
500
1000
1500
-1
0
1
2
3
4
Temperature (Celsius)

Fig. 8

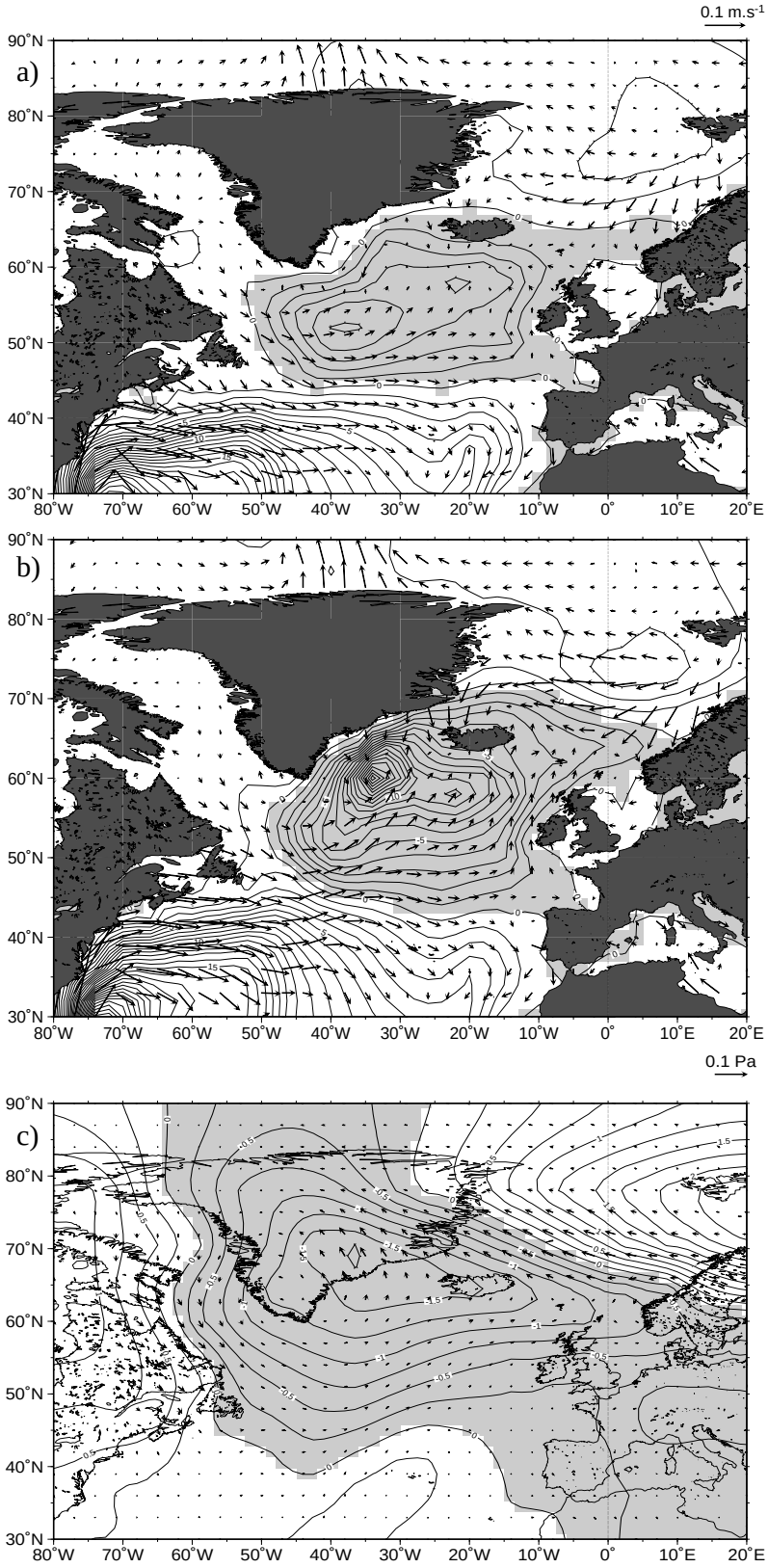
0.1 m.s-1
a)
b)
0.1 Pa
c)
90°N
80°N
70°N
60°N
50°N
40°N
30°N
80°W
70°W
60°W
50°W
40°W
30°W
20°W
10°W
0°
10°E
20°E

Figure 9

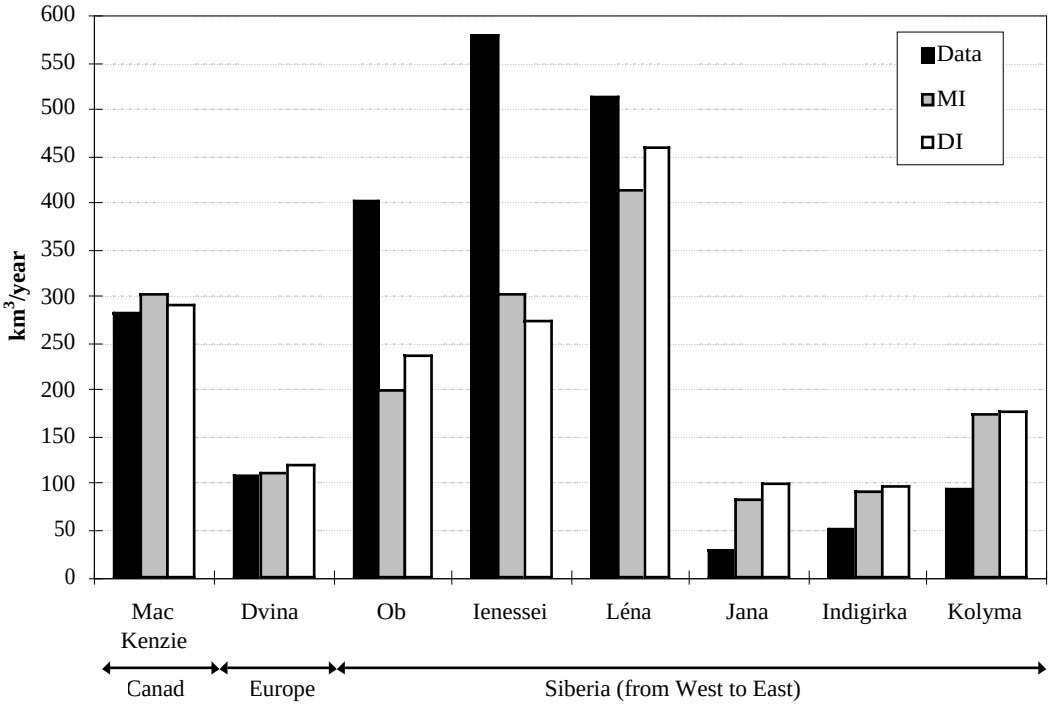
600
550
500
450
400
350
300
250
200
150
100
50
0
km3/year
Data
MI
DI
Mac Kenzie
Dvina
Ob
Ienessei
Léna
Jana
Indigirka
Kolyma
Canad
Europe
Siberia (from West to East)

Fig. 10

Figure 11

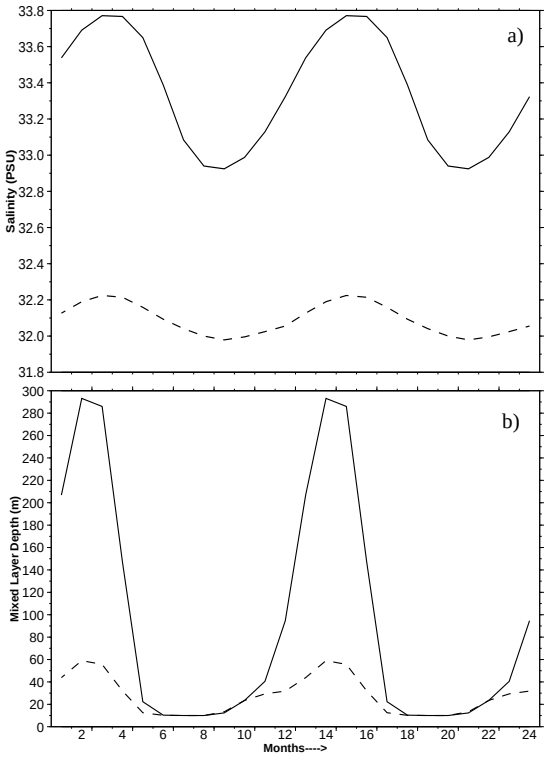

Figure 12

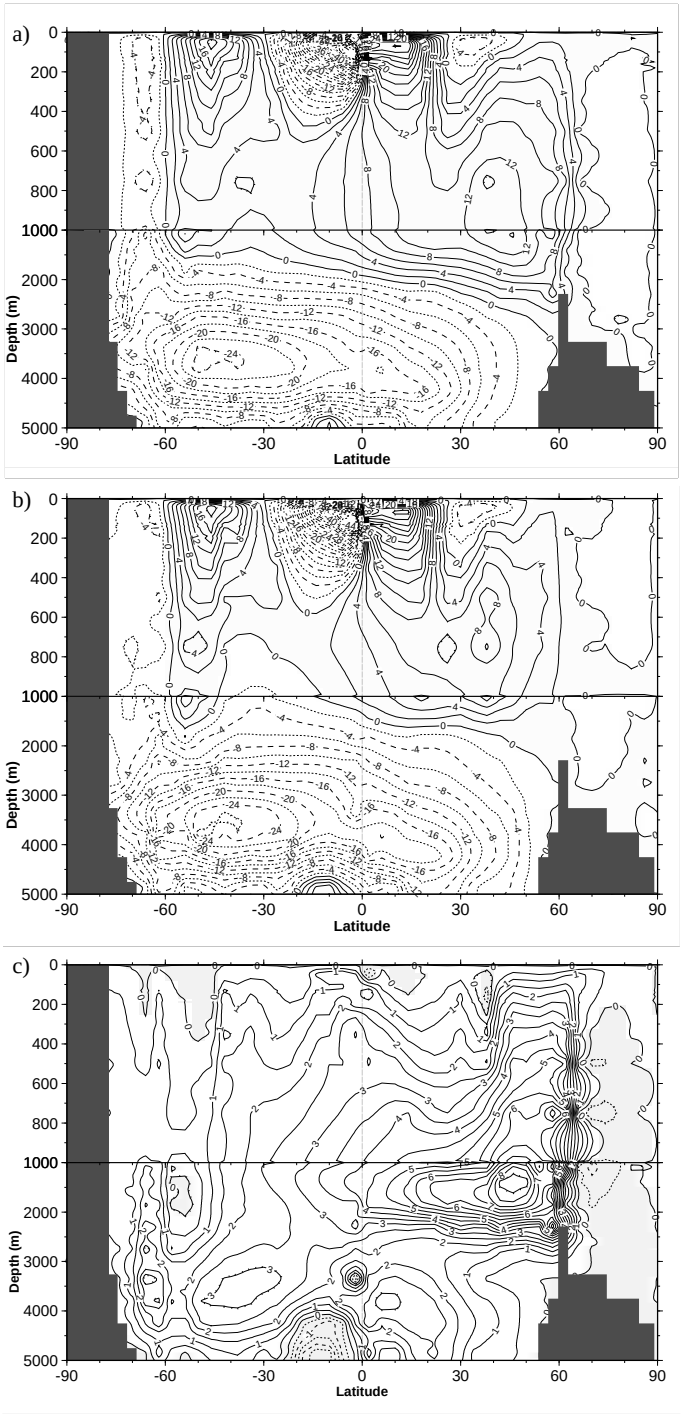

Figure 13

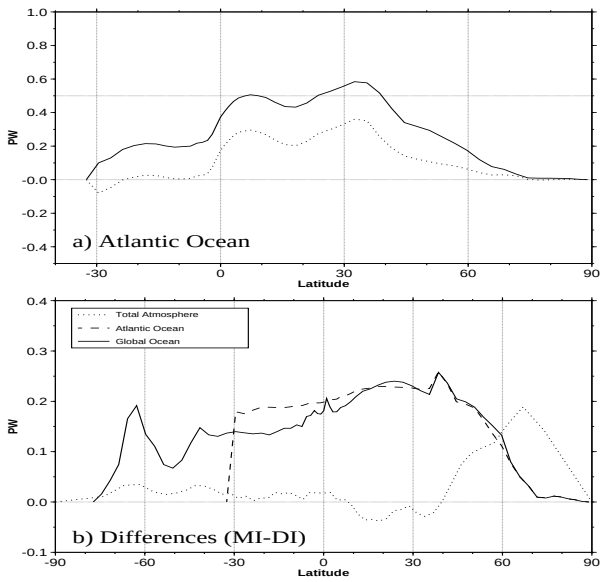

Déjà paru :

9 : Octobre 1998 Francis Codron, Augustin Vintzileos and Robert Sadourny, *An Improved Interpolation Scheme between an Atmospheric Model and Underlying Surface Grids near Orography and Ocean Boundaries.*

10 : Novembre 1998 Z.X. Li and A.F. Carril, *Transient properties of atmospheric circulation in two reanalysis datasets.*

11 : Décembre 1998 Gurvan Madec, Pascale Delecluse, Maurice Imbard and Claire Lévy, *OPA8.1 ocean general circulation model reference manual.*

12 : Janvier 1999 Marc Guyon, Gurvan Madec, François-Xavier Roux, Christophe Herbaut, Maurice Imbard, and Philippe Fraunie, *Domain Decomposition Method as a Nutshell for Massively Parallel Ocean Modelling with the OPA Model .*

13 : Février 1999 Eric Guilyardi, Gurvan Madec, and Laurent Terray, *he Role of Lateral Ocean Physics in the Upper Ocean Thermal Balance of a Coupled Ocean-Atmosphere GCM*

14 : Mars 1999 D. Hauglustaine, *Impact of Biomass Burning and Lightning Emissions on the Distribution of Tropospheric Ozone and its Precursors in the Tropics*

15 : Décembre 1999 L. Menut, R. Vautard, C. Honnoré, and M. Beekmann, *Sensitivity of Photochemical Pollution using the Adjoint of a Simplified Chemistry-Transport Model*

16 : Janvier 2000 J.-Ph. Boulanger, *The Trident Pacific model. Part 1: The oceanic dynamical model and observations during the TOPEX/POSEIDON period*

17 : Janvier 2000 J.-Ph. Boulanger and Christophe Menkes, *The Trident Pacific model Part 2: The thermodynamical model and the role of long equatorial wave reflection during the TOPEX/POSEIDON period*

18 : Octobre 2000 H. Le Treut and B. McAvaney, *A model intercomparison of equilibrium climate change in response to CO_2 doubling*

19 : Octobre 2000 Pierre Friedlingstein, Laurent Bopp, Philippe Ciais, Jean-Louis Dufresne, Laurent Fairhead, Hervé LeTreut, Patrick Monfray, and James Orr, *Positive feedback of the carbon cycle on future climate change*

20 : Février 2001 Agnès Ducharne, Catherine Golaz, Etienne Leblois, Katia Laval, Emmanuel Ledoux, and Ghislain de Marsily, *RiTHM (River Transfer Hydrological Model) : a Runoff Routing Scheme for GCMs*

21 : Octobre 2001 Y. Le Clainche, P. Braconnot, O. Marti, S. Joussaume, J-L. Dufresne, and M-A. Filiberti, *The role of sea ice thermodynamics in the Northern Hemisphere climate as simulated by a global coupled ocean-atmosphere model*

Plus de détails sont disponibles sur Internet :
http://www.ipsl.jussieu.fr/modelisation/liste-notes.html.